12th Symposium of Magnetic Measurements and Modeling SMMM'2016, Częstochowa–Siewierz, Poland, October 17–19, 2016

Magnetic Properties and Phase Constitution of the Nanocrystalline $Fe_{65}Pr_9B_{18}W_8$ Alloy Ribbons

K. Filipecka[a,b,*], P. Pawlik[a], A. Kozdraś[c], J. Filipecki[b], K. Pawlik[a] and J.J. Wysłocki[a]

[a]Institute of Physics, Faculty of Production Engineering and Materials Technology, Czestochowa University of Technology, Armii Krajowej 19, 42-200 Częstochowa, Poland

[b]Institute of Physics, Faculty of Mathematics and Natural Science, Jan Dlugosz University, Armii Krajowej 13/15, 42-200 Częstochowa, Poland

[c]Department of Physics, Faculty of Production Engineering and Logistics, Opole University of Technology, Ozimska 75, 45-370 Opole, Poland

The aim of the present work was to investigate the phase constitution and magnetic properties of the rapidly solidified $Fe_{65}Pr_9B_{18}W_8$ alloy ribbons in the as-cast state and subjected to annealing. The base alloy was prepared by arc-melting of the high purity elements under the Ar atmosphere. The ribbon samples were obtained by the melt-spinning technique under a low pressure of Ar. The studies have shown an amorphous structure of the ribbon in the as-cast state and its soft magnetic properties. Annealing at various temperatures for 5 min resulted in an evolution of the phase constitution that caused changes in magnetic properties of the alloy. The crystallization behavior was studied using differential scanning calorimetry. In order to determine the phase composition of annealed ribbons, X-ray diffractometry was used. The evolution of microstructure and phase constitution was verified by the Mössbauer spectroscopy. The magnetic properties were determined from hysteresis loops measured by a vibrating sample magnetometer in the external magnetic field up to 2 T at room temperature.

DOI: 10.12693/APhysPolA.131.1207

PACS/topics: 75.50.Ww, 75.50.Kj, 71.20.Eh

1. Introduction

RE–Fe–B-type hard magnetic alloys have been subjected to intensive studies since their first announcement in 1984 [1, 2] due to their outstanding properties [3, 4]. These alloys are precursors of permanent magnets, which can be used in a wide range of applications [5–7]. An interesting group are Pr–Fe–B-type alloys, in which the $Pr_2Fe_{14}B$ phase is responsible for the high coercivity [8]. The Pr–Fe–B system is considered as a potentially good candidate as an alternative for the Nd–Fe–B alloys [9]. The $Pr_2Fe_{14}B$ phase does not undergo a spin reorientation down to 4.2 K [10], thus revealing good magnetic properties even at low temperatures. Furthermore, it has a higher value of an anisotropy field (87 kOe) than that for the $N_{d2}Fe_{14}B$ phase (6 kOe) [11]. Therefore, it is expected that Pr replacement will cause the increase of coercivity ${}_JH_c$ and will lead to improvement of the maximum energy product $(\boldsymbol{BH})_{\max}$ [12]. Refinement of the microstructure and modification of the phase constitution by optimizing the chemical composition have an impact on the magnetic properties of Pr–Fe–B-type magnets. The improvement of magnetic parameters can be obtained by changing the proportions of the basic components (Pr, Fe, and B) or by doping with other elements. One of the alloying elements, which has an influence on the microstructure, magnetic properties and improves the glass forming ability of Fe-based alloys is tungsten [13–16]. Furthermore, production method and annealing process are also an important factor in formation of the microstructure and tailoring the magnetic properties. Many manufacturing techniques have been developed for production of hard magnetic materials so far. However, a frequently used method is the melt-spinning of induction molten alloy under controlled atmosphere of Ar, which allows to obtain an amorphous or nanocrystalline ribbons [17, 18]. Further heat treatment allows to control crystallization process and optimize the microstructure and phase composition of alloys. Therefore, in the present work, the influence of annealing conditions on the magnetic properties and the phase composition of the $Fe_{65}Pr_9B_{18}W_8$ nanocrystalline alloy ribbons derived from the amorphous precursors, were investigated.

2. Experimental

The $Fe_{65}Pr_9B_{18}W_8$ alloy ingot sample was prepared by arc-melting of the high purity constituent elements with addition of pre-alloy Fe–B of known composition under an Ar protective atmosphere. In order to homogenize the alloy, the ingot was re-melted several times. Then ribbon samples were produced by single roll melt-spinning technique under the Ar atmosphere (Ar pressure of 0.8 bar). The ingot sample was induction molten in the quartz crucible with the 0.6 mm diameter orifice at its bottom.

*corresponding author; e-mail: kasia.filipecka@onet.eu

The distance between the crucible and the surface of the copper roll was set to 1 mm. The molten alloy was injected on top of the copper roll by the overpressure of argon. The linear velocity of the copper roll surface of 2 m/s was used in the process. Subsequently, the ribbons were sealed off in a quartz tube under low pressure of Ar (0.5 bar) to prevent oxidation during heat treatment. In order to change the magnetic properties and obtain nanocrystalline microstructure, the samples were annealed at various temperatures ranging from 923 K to 1023 K for 5 min, and subsequently rapidly quenched in the water. Crystallization behavior of the as-cast ribbon was studied using Netzsch DSC404 differential scanning calorimeter at the heating rate of 10 K/min. The phase analysis was carried out using Bruker D8 Advance diffractometer with Cu K_α radiation equipped with LynxEye detector (linear focus of 25 mm, primary beam divergent slit — 0.6 mm) with the Soller slits on primary and diffracted beam. The measurements were performed in the Bragg–Brentano configuration with K_β filter on detector side. The 2Θ step size was 0.02 deg and step time 5 s. The Rietveld refinement of X-ray diffraction (XRD) patterns was performed using DIFFRAC Plus TOPAS 4.2 software in 2Θ range from 30 deg to 90 deg to obtain the weight fractions of constituent phases, crystallite sizes and unit cell parameters. The Mössbauer spectra were measured using Polon Mössbauer spectrometer with a ^{57}Co:Rh source in conventional transmission geometry and analyzed using WinNormos for Igor software. Test samples were crushed to powder in order to obtain a specimens representative for the entire volume of the material. Room temperature hysteresis loops were measured using the LakeShore 7307 vibrating sample magnetometer at external magnetic fields up to 2 T.

3. Results and discussion

In order to analyze the crystallization behavior, the differential scanning calorimetry (DSC) curve was measured for the as-cast amorphous ribbon (Fig. 1). It was shown that the crystallization process proceeds in two steps corresponding to the exothermic peaks on the DSC curve. The crystallization temperatures T_{x_1} of 920 K and T_{x_2} of 1020 K were determined from this curve. The DSC studies were used to specify the region of annealing temperatures leading to crystallization.

The XRD patterns measured for the $Fe_{65}Pr_9B_{18}W_8$ alloy ribbons in the as-cast state and annealed at temperatures from 923 K to 1023 K for 5 min, are shown in Fig. 2. For the as-cast sample, a wide bump on XRD pattern in the range of 2Θ from 30 to 50 deg is characteristic for the amorphous phase. Also for the ribbon annealed at 923 K the XRD test did not reveal any changes in the phase constitution. Heat treatment of specimens at the 943 K and higher temperatures led to nucleation and growth of crystalline phases and allowed to obtain a nanocrystalline structure. The volume fraction of the amorphous phase decreased at the expense of growing grains of crystalline

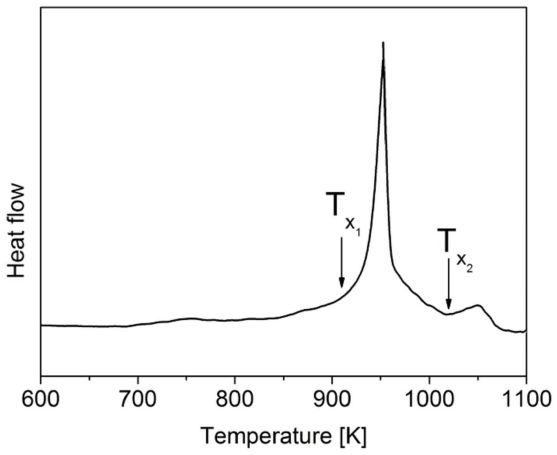

Fig. 1. DSC curves of melt-spun $Fe_{65}Pr_9B_{18}W_8$ ribbon measured at a heating rate of 10 K/min.

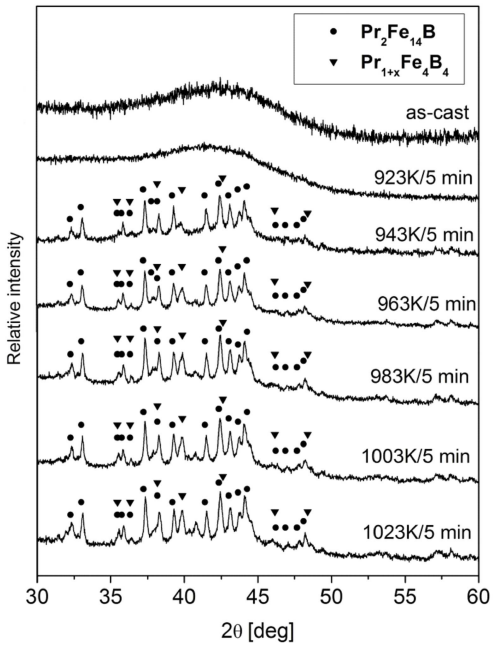

Fig. 2. XRD patterns of rapidly solidified $Fe_{65}Pr_9B_{18}W_8$ alloy ribbons in as-cast state and subjected to annealing at various temperatures for 5 min.

phases. The identified crystalline components precipitating during annealing are the hard magnetic $Pr_2Fe_{14}B$ and the paramagnetic $Pr_{1+x}Fe_4B_4$ phases.

The Rietveld refinement allowed to simulate the unit cell of the constituent crystalline phases and theoretical X-ray pattern and compare it with experimental data (Fig. 3). Additionally, the lattice parameters and volume fractions of constituent phases were determined. The results of the Rietveld refinement of selected samples were collected in Table I. A presence of hard magnetic $Pr_2Fe_{14}B$ and paramagnetic $Pr_{1+x}Fe_4B_4$ crystalline

phases has been taken into account in the refinement (according to XRD and the Mössbauer analysis). The lattice parameters of the constituent phases changed slightly with the annealing temperature. The crystallite sizes of identified phases are of the nanometer size for all phase components. Crystallite sizes calculated for both phases increase with the annealing temperature from 40.4 nm to 55.6 nm for the hard magnetic $Pr_2Fe_{14}B$ phase and from 11.0 nm to 22.1 nm for the paramagnetic $Pr_{1+x}Fe_4B_4$ phase.

TABLE I

Results of the Rietveld refinement carried out for selected samples.

Ann. temp.	Rec. phases	a [Å]	c [Å]	Wt. fr. [wt%]	Cryst. size [nm]
983 K	$Pr_2Fe_{14}B$	8.811	12.231	69.3±2.5	40.4±0.1
	$Pr_{1+x}Fe_4B_4$	6.689	34.210	30.7±2.5	11.0±1.3
1003 K	$Pr_2Fe_{14}B$	8.793	12.212	65.9±1.3	55.6±0.8
	$Pr_{1+x}Fe_4B_4$	6.686	34.453	34.1±1.3	22.1±1.9

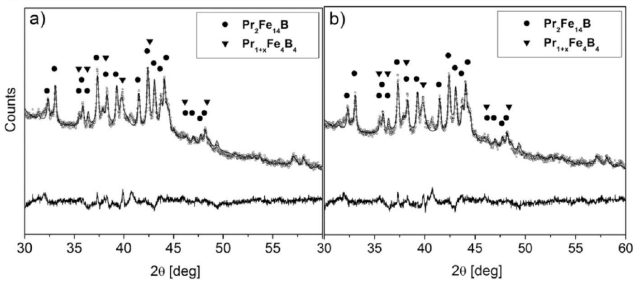

Fig. 3. Rietveld refinement of rapidly solidified $Fe_{65}Pr_9B_{18}W_8$ alloy ribbons annealed at 983 K (a) and 1003 K (b) for 5 min. The experimental data are indicated by dots while the calculated pattern by the overlaying solid line. The difference between the experimental and calculated powder diffraction patterns is shown at the bottom.

The transmission Mössbauer spectra of the $Fe_{65}Pr_9B_{18}W_8$ alloy ribbons in the as-cast state and subjected to annealing are shown in Fig. 4. For the as-cast sample, a wide Mössbauer line corresponding to hyperfine field distribution (HFD) was measured. This indicates disordered surroundings of the Fe atoms in the microstructure that confirms its amorphous structure. Furthermore, the Mössbauer spectra analysis gave information about magnetic properties of the amorphous phase. It was shown that the hyperfine field distribution reaches its maximum at ≈ 16 T. Moreover, the bimodal character of the distribution suggests existence of nonequivalent surroundings of Fe atoms in the amorphous phase. Low values of hyperfine fields around the maxima of HFD suggest weak ferromagnetic ordering in the amorphous phase that results in a low value of its Curie temperature. The Mössbauer spectrum of ribbon annealed at 923 K has shown presence of the

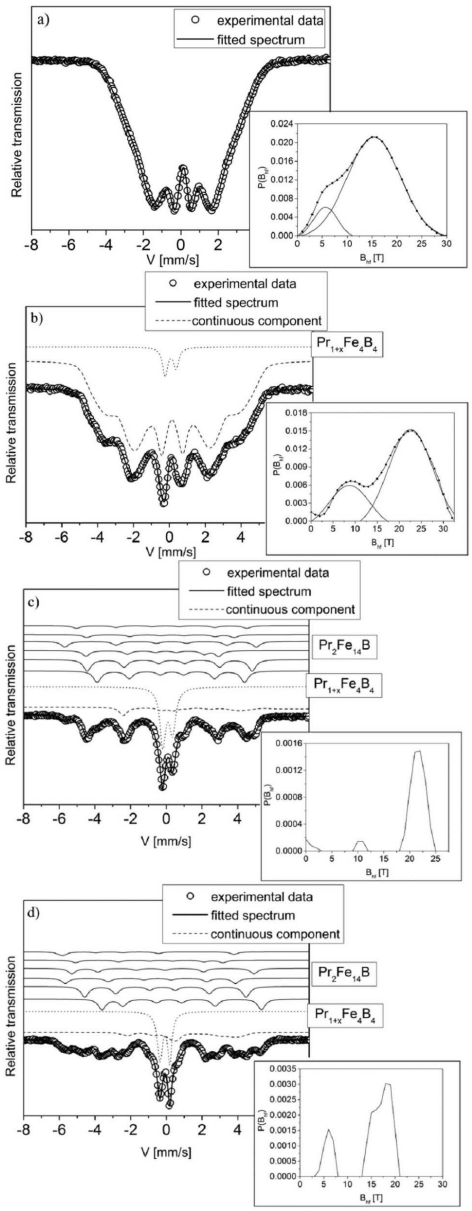

Fig. 4. Transmission Mössbauer spectra with their hyperfine field distributions measured for the $Fe_{65}Pr_9B_{18}W_8$ alloy in as-cast state (a) and annealed at 923 K (b), 983 K (c) and 1003 K (d) for 5 min.

component corresponding only to one paramagnetic crystalline phase and broad sextet defined by hyperfine field distribution. This paramagnetic $Pr_{1+x}Fe_4B_4$ phase was represented by a doublet line in the fitting procedure. Considering the XRD results, the broad sextet can be attributed to the amorphous phase. An alteration of the hyperfine field distribution toward higher fields may suggest a change of the chemical composition of the amorphous matrix. The corresponding volume fractions of constituent phases are 94.4 vol.% of the amorphous and 5.6 vol.% of the $Pr_{1+x}Fe_4B_4$ phase. Low fraction of the $Pr_{1+x}Fe_4B_4$ phase elucidates the

lack of noticeable diffraction peaks in Fig. 2 for the ribbon annealed at 923 K. Annealing at 983 K led to significant changes in the shapes of the Mössbauer spectrum that indicate a presence of a major fraction of crystalline phases. In the fitting procedure, a presence of the paramagnetic $Pr_{1+x}Fe_4B_4$ and hard magnetic $Pr_2Fe_{14}B$ phases (accordingly to XRD studies) were considered. The hard magnetic phase was represented by six Zeeman lines corresponding to the magnetically nonequivalent Fe atom positions in its unit cell (in the Wyckoff notation: $16k_1$, $16k_2$, $8j_1$, $8j_2$, 4e, 4c), for which corresponding line intensities 4:4:2:2:1:1 were arbitrarily set. In order to obtain a good fit, an additional broad sextet line, defined by the hyperfine field distribution was included. A presence of this line can be attributed to the highly disordered $Pr_2Fe_{14}B$ phase formed during short-time annealing and rapid quenching in water. The quantitative analysis of this spectra has shown that with the increase of annealing temperature the volume fraction of hard magnetic phase increases at the expense of paramagnetic $Pr_{1+x}Fe_4B_4$ phase.

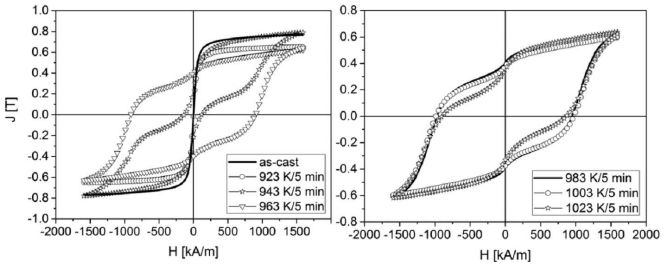

Fig. 5. The hysteresis loops measured for rapidly solidified $Fe_{65}Pr_9B_{18}W_8$ alloy ribbons in as-cast state and subjected to annealing at various temperatures for 5 min.

TABLE II

Magnetic parameters: coercivity field ${}_JH_c$, remanence polarization J_r and maximum energy product $(\boldsymbol{BH})_{\max}$ for annealed ribbon samples.

Annealing temperature [K]	${}_JH_c$ [kA/m]	J_r [T]	$(\boldsymbol{BH})_{\max}$ [kJ/m^3]
923	2	0.02	–
943	136	0.25	2.9
963	896	0.40	22.3
983	955	0.39	23.3
1003	974	0.37	20.1
1023	876	0.34	15.1

The hysteresis loops of the $Fe_{65}Pr_9B_{18}W_8$ alloy ribbons in the as-cast state and annealed at temperatures from 923 K to 1023 K for 5 min, are shown in Fig. 5. Magnetic measurements carried out on as-cast ribbon have shown its soft magnetic properties (Fig. 2a). A similar shape of the hysteresis loop measured for ribbon annealed at 923 K also proves only precipitation of a paramagnetic phase within the amorphous matrix. The wasp-waisted shape of the hysteresis loop measured for the ribbon annealed at 943 K is typical for alloys, where formation of isolated grains of a hard magnetic phase within the amorphous matrix occurs during the heat treatment. With the increase of annealing temperature, hysteresis loops characteristic for hard magnetic materials were measured which are related to an evolution of microstructure and the phase constitution of the samples. Large volume fraction of the paramagnetic $Pr_{1+x}Fe_4B_4$ phase and change of the chemical composition of the amorphous matrix resulted in relatively low values of $(\boldsymbol{BH})_{\max}$. With the rise of the annealing temperature, a slight increase of the coercivity is observed. The maximum value of coercivity ${}_JH_c = 974$ kA/m was measured for the a sample annealed at 1003 K, however the maximum values of remanence $J_r = 0.39$ T and maximum energy product $(\mathrm{BH})_{max} = 23.3$ kJ/m^3 were determined for the ribbon annealed at 983 K for 5 min. The basic magnetic properties of the $Fe_{65}Pr_9B_{18}W_8$ alloy ribbons were collected in Table II. Annealing at 1023 K resulted in deterioration of the magnetic properties. This may be related to crystallization of an additional phase (indicated by the DSC measurements) accompanied by reduction of volume fraction of the hard magnetic phase.

4. Conclusions

XRD has shown that $Fe_{65}Pr_9B_{18}W_8$ alloy ribbons in the as-cast state had amorphous structure. Annealing at 923 K for 5 min resulted in partial crystallization of specimen. The Mössbauer spectroscopy has shown that annealing led to precipitation of the paramagnetic $Pr_{1+x}Fe_4B_4$ phase within the amorphous matrix. Low fraction of this phase elucidates the lack of noticeable diffraction peaks. Both as-cast and annealed (at 923 K) ribbons were soft magnetic. Furthermore, the Mössbauer spectra analysis has shown the bimodal character of the hyperfine field distribution, suggesting the existence of nonequivalent surroundings of Fe atoms in the amorphous phase. Low values of maxima of hyperfine field distribution imply weak ferromagnetic ordering in the amorphous phase. For the ribbon annealed at 923 K, an alteration of the hyperfine field distribution toward higher fields may suggest changes in the chemical composition of the amorphous matrix. Heat treatment of ribbons at 943 K and higher temperatures led to the nucleation and growth of the hard magnetic $Pr_2Fe_{14}B$ and the paramagnetic $Pr_{1+x}Fe_4B_4$ phases. The Rietveld refinement of XRD patterns had shown that nanocrystals of identified phases were formed. Calculated unit cell parameters of the constituent phases changed slightly with annealing temperature. With the increase of annealing temperature the crystallite size increased from 40.4 nm to 55.6 nm for the hard magnetic $Pr_2Fe_{14}B$ phase, while for the paramagnetic $Pr_{1+x}Fe_4B_4$ the crystallite average size increased from 11.0 nm to 22.1 nm. Moreover, large fraction of the hard magnetic $Pr_2Fe_{14}B$ phase crystal-

lized during annealing. The rise of annealing temperature caused an increase of hard magnetic parameters of investigated ribbons. Heat treatment at 1023 K resulted in deterioration of the magnetic properties, which may be caused by the crystallization of an additional phase (indicated by the DSC measurements) accompanied by a reduction of the volume fraction of the $Pr_2Fe_{14}B$ phase. Relatively low values of $(\boldsymbol{BH})_{\max}$ measured for annealed samples are related to a high volume fraction of the paramagnetic $Pr_{1+x}Fe_4B_4$ phase. The maximum value of coercivity ${}_JH_c = 974$ kA/m was obtained for the sample annealed at 1003 K for 5 min. However, annealing at 983 K for 5 min resulted in the maximum values of remanence $J_r = 0.39$ T and maximum energy product $(\boldsymbol{BH})_{\max} = 23.3$ kJ/m^3.

References

[1] M. Sagawa, S. Fujimura, N. Togawa, H. Yamamoto, *J. Appl. Phys.* **55**, 2083 (1984).

[2] J.J. Croat, J.F. Herbst, R.E. Lee, F.E. Pinkerton, *J. Appl. Phys.* **55**, 2078 (1984).

[3] S. Hirosawa, in: *Concise Encyclopedia of Magnetic and Superconducting Materials*, Ed. K.H.J. Buschow, Elsevier, Amsterdam 2005.

[4] D.C. Jiles, *Acta Mater.* **51**, 5907 (2003).

[5] R. Skomski, J.M.D. Coey, *Permanent Magnetism*, Taylor & Francis Group, New York 1999.

[6] W. Liu, Y. Liu, R. Skomski, D.J. Sellmyer, in: *Handbook of Advanced Magnetic Materials*, Eds. Y. Liu, D. Sellmyer, D. Shindo, Tsinghua University Press-Springer, New York 2006.

[7] Y. Matsuura, *J. Magn. Magn. Mater.* **303**, 34 (2006).

[8] J.H. Herbst, W.B. Yelon, *J. Appl. Phys.* **57**, 2343 (1985).

[9] E.B. Boltich, E. Oswald, M.Q. Haung, S. Hirosawa, *J. Appl. Phys.* **57**, 4106 (1985).

[10] E.B. Boltich, W.E. Wallace, *Solid State Commun.* **55**, 529 (1985).

[11] S. Hirosawa, Y. Matsuura, H. Yamamoto, *J. Appl. Phys.* **59**, 873 (1986).

[12] D.H. Ping, T.S. Xie, D.X. Li, H.Q. Ye, *Nanostruct. Mater.* **5**, 457 (1995).

[13] K. Filipecka, P. Pawlik, A. Kozdras, J. Filipecki, *Acta Phys. Pol. A* **129**, 185 (2016).

[14] K. Filipecka, P. Pawlik, K. Pawlik, P. Gębara, A. Przybył, M. Pruba, *Acta Phys. Pol. A* **128**, 104 (2015).

[15] B. Xiaoqian, Z. Jie, L. Wei, G. Xuexu, Z. Shouzeng, *J. Rare Earth* **27**, 843 (2000).

[16] A. Przybył, J.J. Wysłocki, *J. Mater. Process. Technol.* **175**, 352 (2006).

[17] K. Filipecka, P. Pawlik, J. Filipecki, *J. Alloys Comp.* **694**, 228 (2017).

[18] M. Szwaja, P. Gębara, J. Filipecki, K. Pawlik, A. Przybył, P. Pawlik, J.J. Wysłocki, K. Filipecka, *J. Alloys Comp.* **382**, 307 (2015).